nature materials

ARTICLES

https://doi.org/10.1038/s41563-019-0586-y

Fatigue of graphene

Teng Cui[1,4], Sankha Mukherjee[2,4], Parambath M. Sudeep[1], Guillaume Colas[1], Farzin Najafi[1], Jason Tam[2], Pulickel M. Ajayan[3], Chandra Veer Singh[2*], Yu Sun[1*] and Tobin Filleter[1*]

Materials can suffer mechanical fatigue when subjected to cyclic loading at stress levels much lower than the ultimate tensile strength, and understanding this behaviour is critical to evaluating long-term dynamic reliability. The fatigue life and damage mechanisms of two-dimensional (2D) materials, of interest for mechanical and electronic applications, are currently unknown. Here, we present a fatigue study of freestanding 2D materials, specifically graphene and graphene oxide (GO). Using atomic force microscopy, monolayer and few-layer graphene were found to exhibit a fatigue life of more than 10^9 cycles at a mean stress of 71 GPa and a stress range of 5.6 GPa, higher than any material reported so far. Fatigue failure in monolayer graphene is global and catastrophic without progressive damage, while molecular dynamics simulations reveal this is preceded by stress-mediated bond reconfigurations near defective sites. Conversely, functional groups in GO impart a local and progressive fatigue damage mechanism. This study not only provides fundamental insights into the fatigue enhancement behaviour of graphene-embedded nanocomposites, but also serves as a starting point for the dynamic reliability evaluation of other 2D materials.

Fatigue failure of materials has long been a major concern, and research on fatigue can be traced back to the early nineteenth century[1]. Because fatigue can occur at stress levels much lower than the static fracture strength[2], investigating fatigue behaviour and the underlying damage mechanisms is critical for the application of an emerging material in order to evaluate its long-term reliability. Two-dimensional (2D) materials have been widely applied to mechanical and electronic applications, where they are commonly subjected to cyclic stress[3–8]. However, at the limit of these atomically thin materials, it is not clear if they exhibit the fatigue phenomenon. If they do, then the following open questions arise: what are the fatigue lifetimes and what are the underlying damage mechanisms? Despite a lack of knowledge about the intrinsic fatigue behaviour of 2D materials such as graphene, macroscopic studies have already demonstrated that adding even a small amount (<1 wt%) of graphene can improve the fatigue life of polymer-based composites by ~1–2 orders of magnitude[9–11].

Atomic force microscopy-based fatigue testing

A modified atomic force microscopy (AFM) technique, which enables application of a combination of both static and cyclic mechanical loading to a suspended 2D film, was developed to study the fatigue properties of graphene. The approach for applying static loading is similar to that used in traditional AFM deflection tests for measuring the static mechanical properties (for example, Young's modulus and intrinsic strength) of suspended graphene[12,13]. As illustrated in Fig. 1a (see also Supplementary Fig. 1), a certain predefined static force is first applied and maintained at the centre of the film, and then the AFM cantilever is oscillated by a shake piezo around the static deflection at a prescribed frequency and amplitude. Analogous to the direct/alternating current of electricity, the static and cyclic forces are termed d.c. (F_{dc}) and a.c. (F_{ac}) forces. By changing the driving frequency (f_0) and driving amplitude (A_0), the responsive tip deflection amplitude (A_1) is tuned. In the experiment, F_{dc} and A_1 were varied in a controlled manner to allow fatigue testing at different mean stress levels and stress amplitudes (Supplementary Fig. 2). The onset of fatigue failure was determined by the abrupt change in the cantilever tip amplitude

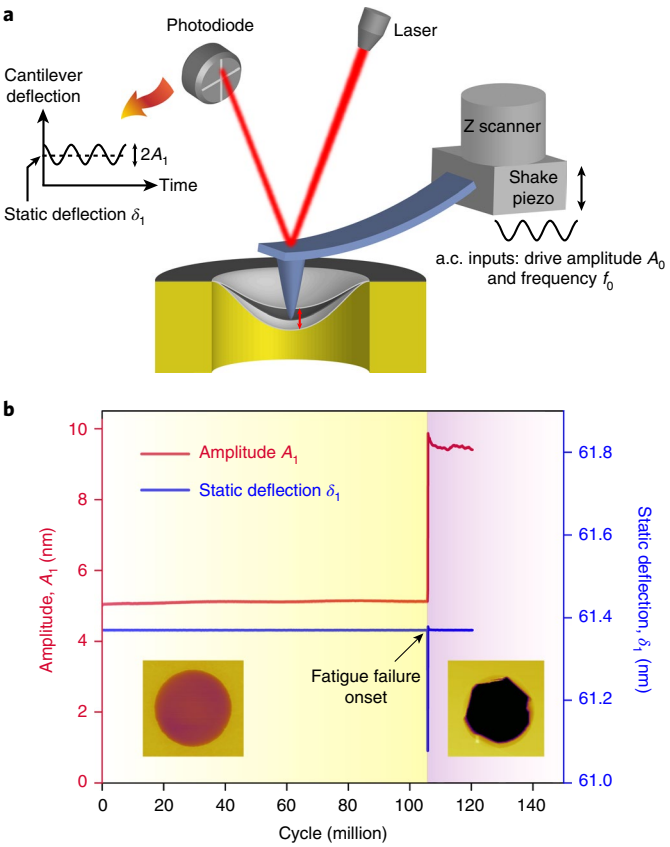

Fig. 1 | Fatigue testing of 2D materials. a, Schematic of the fatigue testing set-up. **b**, Experimental data showing evolution of the amplitude and d.c. force signals. Abrupt jumps of the amplitude and d.c. deflection signals indicate the onset of fatigue failure in the film after ~106 million cycles. Insets: AFM topographic images before and after fatigue failure. Sample diameter, 2.5 μm.

[1]Department of Mechanical and Industrial Engineering, University of Toronto, Toronto, Ontario, Canada. [2]Department of Materials Science and Engineering, University of Toronto, Toronto, Ontario, Canada. [3]Department of Materials Science and NanoEngineering, Rice University, Houston, TX, USA. [4]These authors contributed equally: Teng Cui, Sankha Mukherjee. *e-mail: chandraveer.singh@utoronto.ca; sun@mie.utoronto.ca; filleter@mie.utoronto.ca

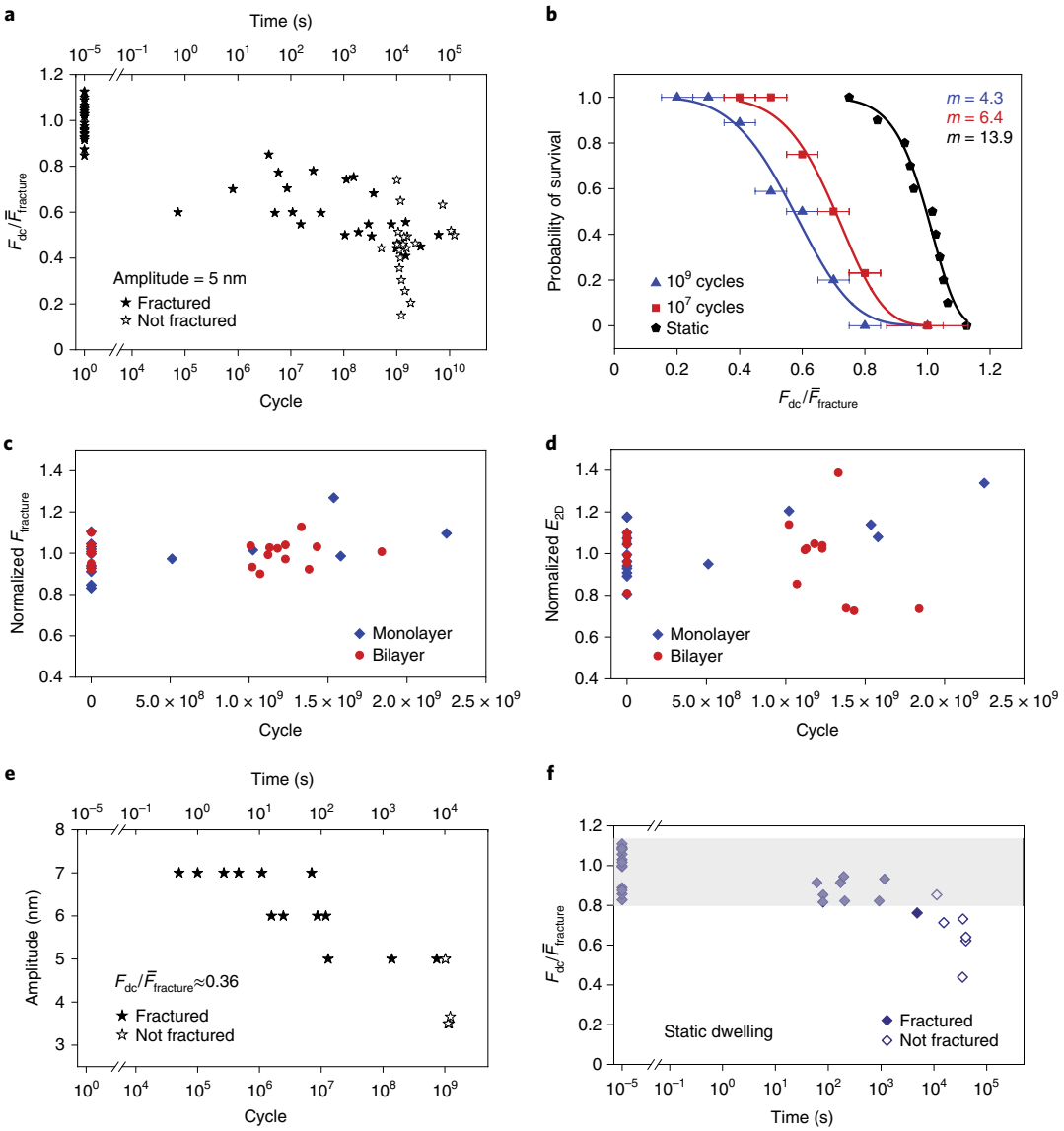

Fig. 2 | Fatigue of graphene. a, $F_{dc}/\bar{F}_{fracture}$–$N$ curve of graphene (2.5 μm diameter, 5 nm tip amplitude), showing a longer lifetime at lower mean stress. **b**, Probability of survival for graphene under static and cyclic loading. **c**,**d**, Normalized fracture force (**c**) and elastic modulus (**d**) of monolayer and bilayer graphene after fatigue loading at 50% of its static fracture force and 5 nm amplitude for various cycles. The properties are normalized by the average properties of the pristine samples without fatigue loading. **e**, Cyclic loading of graphene (1.5 μm diameter) at different amplitudes under fixed d.c. force ($F_{dc}/\bar{F}_{fracture} \approx 0.36$), showing a longer lifetime at lower amplitude. **f**, Long-term static dwelling of graphene, showing fracture at close to its static fracture strength. No fracture was observed below $F_{dc}/\bar{F}_{fracture} \approx 0.76$ within the equivalent time of reaching more than one billion (up to four billion) cycles of loading.

and static deflection signals. Figure 1b shows one representative set of experimental fatigue results on a bilayer graphene sample under static loading of 50% of its fracture force, coupled with cyclic loading of 5 nm amplitude. An abrupt jump of the amplitude and d.c. deflection signals indicates the onset of fatigue failure in the film after ~106 million cycles, which was also confirmed by post-fatigue AFM topographic imaging.

Fatigue behaviour was characterized for three groups of samples (Supplementary Figs. 3 and 4): mechanically exfoliated graphene (<5 layers, including monolayer), GO (<5 layers, including monolayer) and thick multilayer GO (approximately tens of layers). Single-crystal diamond AFM probes were used to mitigate wear of the probe during fatigue testing. Fatigue characterization of graphene (75 samples), GO (12 samples) and thick multilayer GO (19 samples) was conducted at varying F_{dc} levels with a constant tip oscillation frequency of 100 kHz. The effect of amplitude was also investigated through experiments with varying deflection amplitude (A_1). Given that the utility of direct stress measurements is controversial for multilayer films, especially for GO because of its elastoplastic nature and local thickness heterogeneity[14,15], the F_{dc} values reported here were normalized by the average quasi-static fracture force ($\bar{F}_{fracture}$) for each sample group to allow a relative comparison of the fatigue life for samples with varying thicknesses. Representative quasi-static force–deflection curves for graphene and GO are shown in Supplementary Fig. 5. Following an approach analogous to the stress (S)–cycle (N) curves used for the analysis of conventional macroscopic fatigue experiments, a normalized $F_{dc}/\bar{F}_{fracture}$–$N$ plot (hereafter referred to as F–N plots for brevity) for graphene is provided in Fig. 2a. Data at the 10^0 cycle represent multiple measurements of the static fracture force

normalized by the average fracture force. The AFM instrument was operated in an acoustic enclosure to reduce ambient vibrations. The relative humidity in the enclosure was kept in the small range of 28–32% to minimize potential property changes due to ambient humidity fluctuations.

Fatigue behaviour of graphene

The *F*–*N* curve for graphene (Fig. 2a) revealed a significant increase in fatigue life from 10^5 to more than 10^9 cycles when F_{dc} was reduced from ~80% of $\bar{F}_{fracture}$ to ~50% of $\bar{F}_{fracture}$. Open symbols indicate cases where no failure had occurred by the end of testing. For graphene with 2.5 μm diameter, this represents a mean stress of 71 GPa and a stress range of 5.6 GPa at 50% of the static fracture force and 5 nm tip amplitude based on nonlinear finite element analysis (FEA; Supplementary Fig. 6). No other materials have been reported with more than 10^9 cycles of fatigue life at such high mean stresses and stress amplitudes. Such stress levels are at least an order of magnitude higher than those in most macroscopic fatigue tests on high-strength steels and aerospace aluminium alloys[16,17]. Previous studies[18–21] on nanowires showed fewer than 10^6 cycles of fatigue life at ~0.5 GPa stress amplitude (Ni nanowires) or more than 10^9 cycles but at orders of magnitude lower mean stress and stress amplitude primarily achieved through resonance oscillation (ZnO nanowires). The fatigue life of ultrathin (submicrometre) metallic films (for example, Cu or Au)[22–24] revealed a strong dependence on thickness and grain size, but all exhibited lower fatigue resistance than graphene. Other nanoscale fatigue measurements, including AFM-based cyclic bending on Si and SiO_2 nanobeams[25,26], revealed lifetimes of a few thousand to approximately one million cycles at mean stresses and stress amplitudes of a few GPa. Other carbon polymorphs, such as graphite and bulk chemical-vapour-deposited (CVD) diamond, have also been demonstrated to survive more than 10^9 and 10^7 cycles, respectively, but at stress levels of less than 1 GPa (refs. [27,28]). Interestingly, single-crystalline diamond nanoneedles revealed ultra-large elastic deformation and tensile strength due to a paucity of defects[29], which poses the question of whether defect-free diamond could also possess similar ultrahigh fatigue life at large stress levels, like graphene.

The fatigue data are scattered at high stress levels, primarily due to the stochastic nature of brittle failure in graphene. To better understand this stochastic behaviour, we conducted a Weibull statistical analysis on the survival probability of graphene under fatigue loading for different cycles, and compared this with the quasi-static failure case. A two-parameter Weibull distribution is widely used to describe the failure or survival of materials under different loading conditions, both statically and cyclically[12,30–32].The probability of survival at a given force *F*, normalized by the average quasi-static breaking force $\bar{F}_{fracture}$, is given by

$$S = \exp\left[-\left(\frac{F/\bar{F}_{fracture}}{\lambda}\right)^m\right]$$

where *m* is the Weibull modulus, which determines the breadth of the probability distribution, and λ is a nominal ratio associated with the distribution. A larger *m* generally indicates that the failure is less sensitive to the presence of defects, or that there is a small range of defects. The graphene samples in this work were mechanically exfoliated and are known to have low defect density. In Fig. 2b, the Weibull modulus of the static loading case is 13.9, which is close to the value obtained in ref. [12] ($m \approx 16$), confirming the high quality of the graphene. In comparison, the values ot Weibull modulus for graphene to survive 10^9 and 10^7 cycles are 4.3 and 6.4, respectively. The lower Weibull moduli for the fatigue cases suggest that the structure is more sensitive to defects under cyclic loading than under quasi-static loading. The sensitivity to defects is higher if graphene needs to survive more (10^9) rather than fewer (10^7) cycles.

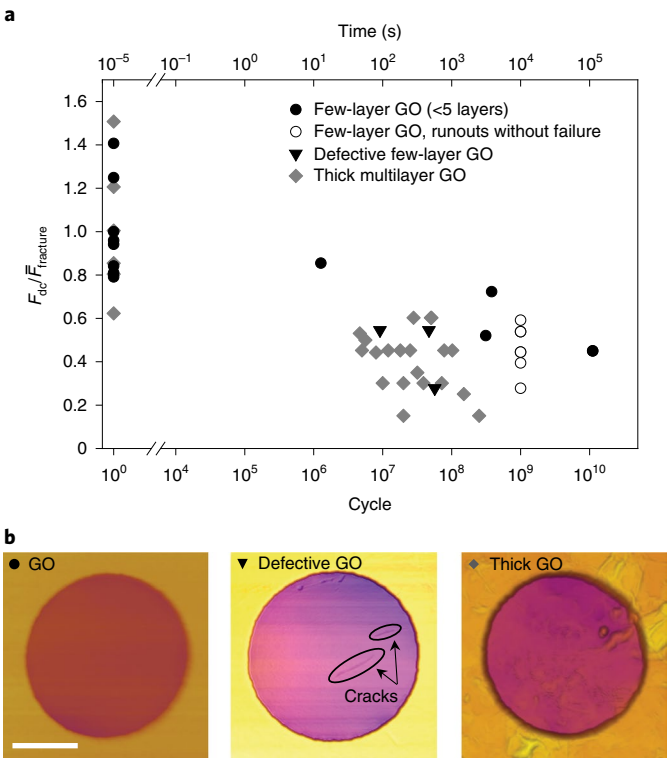

Fig. 3 | Fatigue of GO. a, $F_{dc}/\bar{F}_{fracture}$–*N* curves showing at least one order of magnitude difference in fatigue life between few-layer GO and thick GO due to the presence of critical defects. **b**, AFM topographic images of GO, defective GO and thick GO. Scale bar, 1 μm.

The horizontal scale bars for the fatigue data points represent the ±0.05 range considered for the probability calculation.

The quasi-static mechanical properties of graphene were recharacterized after surviving cyclic loading for different numbers of cycles, as shown in Fig. 2c,d. For both monolayer and bilayer graphene, the results reveal that, after more than one billion cycles of loading at ~50% of fracture force and 5 nm amplitude, there is no degradation in their quasi-static strength and elastic modulus. The larger scatter in the elastic modulus for bilayer graphene is caused by cyclic loading-induced wrinkling and local delamination, while no morphological change was observed for monolayer graphene (both are shown in Supplementary Fig. 7). All the graphene data show that monolayer graphene either fails catastrophically or remains unchanged after cyclic loading, which does not lead to obvious progressive damage/plasticity. Despite the fact that the graphene–graphene interface dissipates energy, bilayer and few-layer graphene still demonstrate more than one billion cycles of fatigue life at large stress levels.

The fatigue life of graphene was observed to be strongly dependent on the stress amplitude. The results in Fig. 2e show that the graphene films cyclically loaded with 7 nm tip amplitude ($\Delta\sigma = 22.4$ GPa) exhibited two orders of magnitude shorter lifetime than those loaded with a 5 nm amplitude ($\Delta\sigma = 16.1$ GPa) under a fixed d.c. force ($F_{dc}/\bar{F}_{fracture} = 0.36$, $\sigma_{mean} = 53.3$ GPa). A tip oscillation amplitude of 3.5 nm ($\Delta\sigma = 11.0$ GPa) consistently allowed more than one billion cycles of fatigue life. The FEA results demonstrate that the friction and local sliding at the graphene–diamond tip interface have a limited effect (<6%) on the stress range of graphene during cyclic loading, and the effect is consistent for different amplitudes (Supplementary Fig. 8). To further understand the cyclic loading effect, a comparison was also made with long-term static

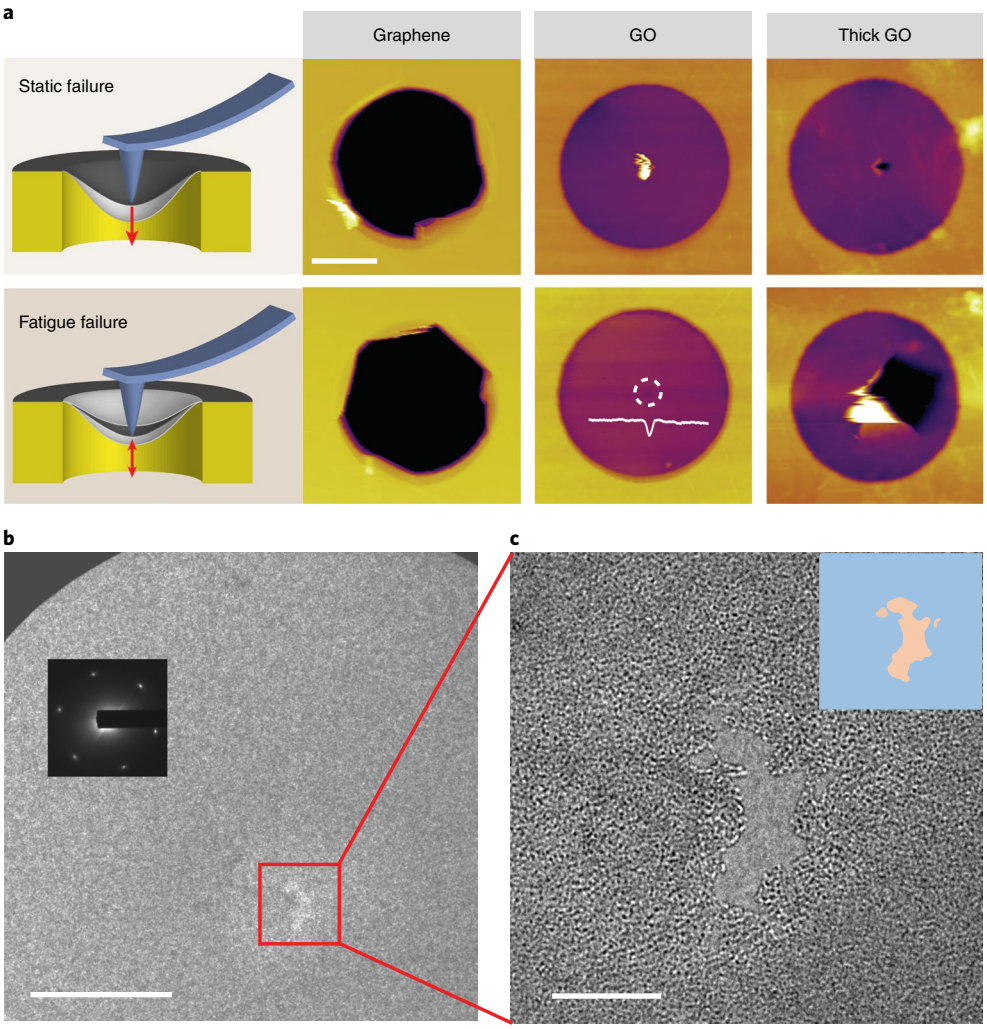

Fig. 4 | Fatigue fracture morphology. a, AFM topographic images of fracture surfaces of graphene, GO and thick GO under static and fatigue loading to failure. **b**,**c**, TEM images of the local fatigue fractured zone for monolayer GO. Insets: selected area electron diffraction pattern showing one set of six diffraction spots (**b**) and a false-colour image of the fracture surface (**c**). Scale bars, 1 μm (**a**), 500 nm (**b**) and 100 nm (**c**).

dwelling of graphene, in which only thermal fluctuations contribute to a near zero (<15 pm) tip amplitude. As revealed in Fig. 2f, graphene can also exhibit fracture under long-term static dwelling; however, in such instances, fracture only ever occurred for cases close to the static fracture force. Within the equivalent time of reaching more than one billion cycles, no static fracture was observed for force ratios below ~0.76, while the cyclic loading resulted in fracture at force ratios as low as ~0.4 (Fig. 2a,e). Previous studies[33–36] on the kinetics of fracture of solids suggested that the nature of bond breaking is caused by thermal fluctuations, and applying a tensile stress could excite the bond and reduce the activation barrier for fracture. Such long-term static loading on atomically thin graphene in our study directly revealed that thermal fluctuations can indeed cause covalent bond fracture with the aid of applied stress below the quasi-static fracture strength (Fig. 2f). Furthermore, the comparison of the lifetimes for cyclic and equivalent long-term static loading suggests that mechanical oscillation can further reduce the activation barrier for chemical bond breaking, which increases the probability of fracture, thus reducing the lifetime. However, further study is still required to gain a deeper insight into the kinetics of dynamically induced chemical bond fracture for such nanoscale materials.

Fatigue behaviour of functionalized graphene

In the case of GO, Fig. 3a also shows increasing fatigue life with reduced static loading force for both few-layer and thicker films, but the increase is less dramatic than for graphene. The few-layer GO samples exhibited more than 10^9 cycles of fatigue life at a force ratio below ~60%, which is at least one order of magnitude longer lifetime than for thick GO samples. This significant discrepancy in fatigue life between few-layer and thick GO can be attributed to a higher probability of the presence of critical defects in the thicker GO films. Abundant wrinkles, folds and partial layer intercalation were observed in thick GO samples (Fig. 3b and Supplementary Fig. 4d) and lead to a local thickness variation. Such local thickness heterogeneity results in stress concentration near the inner edges[15], thus contributing to local crack initiation and propagation. To confirm whether the presence of critical defects is a determinant of the shorter fatigue life of thick multilayer GO films, fatigue testing was also conducted on few-layer GO that had pre-existing major defects, for example, on samples with natural pre-cracks (Fig. 3b). The fatigue life of such defective few-layer GO was measured to fall back into the regime populated by thick multilayer GO films.

The fracture morphologies of graphene and GO under static and fatigue loading were observed to differ significantly (Fig. 4a).

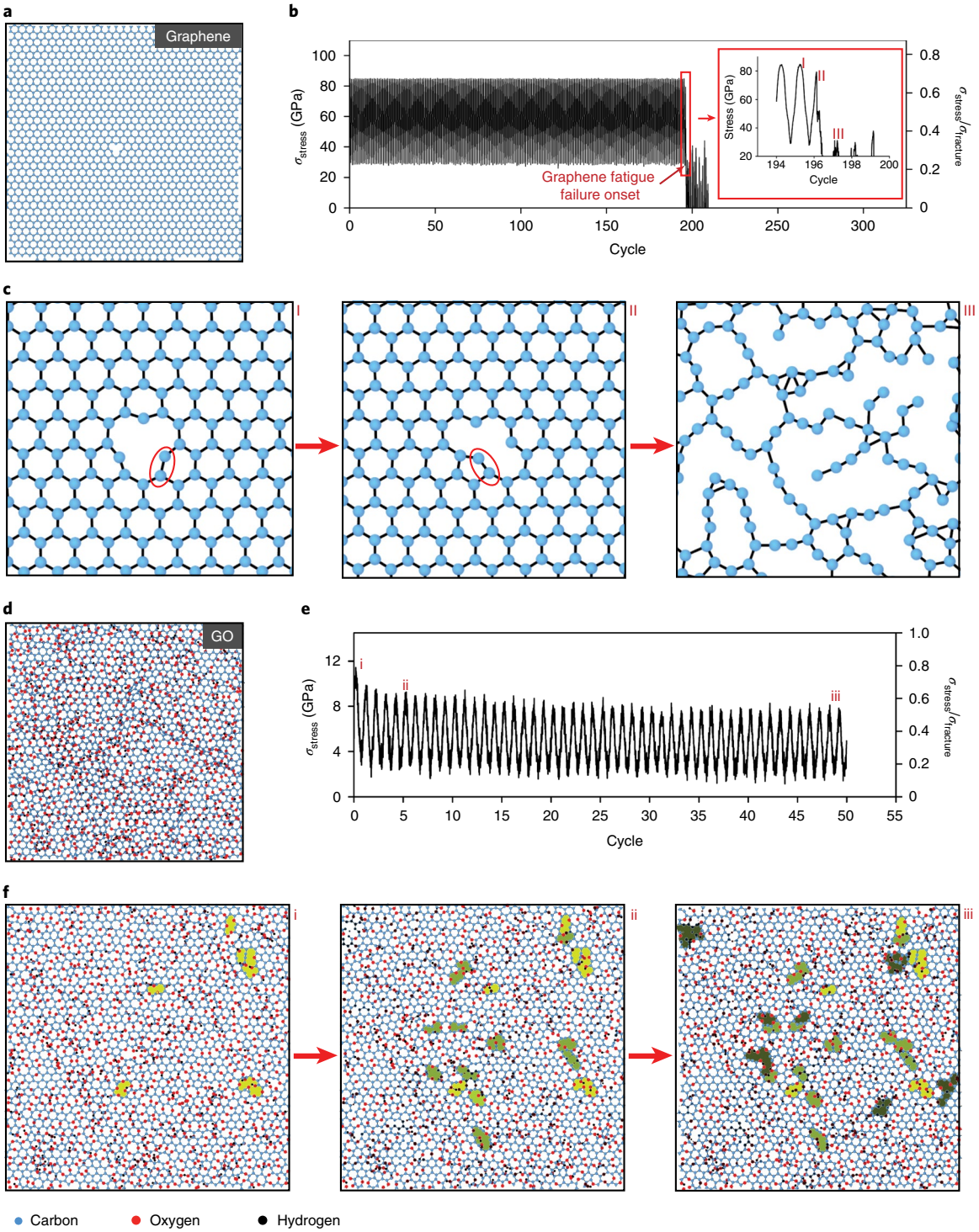

Fig. 5 | MD fatigue simulations of graphene and GO. a, Graphene MD model with a single vacancy defect. **b**, Graphene stress profile during fatigue loading. Inset: enlarged image of the stress profile near fracture onset. **c**, Morphology of graphene at three different cycles labelled in **b**, showing bond reconfiguration at the defective site followed by catastrophic failure. **d**,**e**, GO MD model with a single vacancy defect and the stress profile during fatigue loading. **f**, Progressive damage morphology of GO at the different fatigue cycles labelled in **e**. Major defects are shown in green, with darker green identifying defects generated in later cycles.

Graphene was found to fail globally and catastrophically under both static and fatigue loading scenarios. In contrast, monolayer and few-layer GO films without critical defects exhibited localized failure for both loading conditions, consistent with their elastoplastic mechanical behaviour[14]. Interestingly, thick multilayer GO demonstrated local failure under quasi-static loading, but consistently exhibited a more global fractured zone under fatigue, which can be attributed to the progressive damage during dynamic loading because of the existence of multiple layers and potentially a higher number of critical defects (Supplementary Fig. 4d). In addition, the fatigue damage zone of monolayer GO was also examined by transmission electron microscopy (TEM), as shown in Fig. 4b,c. The localized fracture zone can be explained by the crack-arresting mechanism of oxygen-containing functional groups[37]. When pre-existing critical defects

(for example, cracks) were present in few-layer GO films, their fatigue failure probably initiated at the defective sites and thus they exhibited a larger damage zone (Supplementary Fig. 9).

Atomistic insights on fatigue mechanisms

Molecular dynamics (MD) simulations were conducted to further understand the atomistic mechanisms underpinning fatigue failure. The interatomic interactions were captured using the ReaxFF potential[37–39], as this reactive bond order potential can properly capture bond breaking. Equibiaxial cyclic straining of graphene and GO was performed to mimic experimental loading conditions. The samples were first stretched by a mean tensile strain followed by cyclic straining, which kept the material in tension globally during the fatigue process. Considering sample imperfections as present in experiments, a single vacancy defect was introduced into both the graphene and GO (Fig. 5a,d). Abrupt and catastrophic fatigue failure of graphene was observed at stress levels close to its static fracture stress ($\sigma_{fracture}$), similar to previous observations[40]. It was also shown that cyclic loading results in a shorter lifetime than static dwelling, and higher amplitude gives rise to earlier fracture than lower amplitude (Supplementary Fig. 10c), which agrees with the experimental observations (Fig. 2e,f). A typical example, shown in Fig. 5b for graphene, demonstrates that no progressive stress loss occurred until fatigue failure onset at ~200 cycles, after which the stress dropped abruptly. One major reason for the much shorter fatigue life in MD than experiments is the significant discrepancy in stress amplitude, on which the lifetime strongly depends (Fig. 2e). Furthermore, it was consistently observed that the failure of monolayer graphene was preceded by bond reconfiguration at the vacancy defect. The bond reconfiguration refers to the breaking of an existing bond and bond reconstruction with other atoms due to atom migration, as shown in Fig. 5c (see also Supplementary Videos 1 and 2). The bond reconfiguration near the defect is attributed to the inhomogeneous charge distribution and higher potential energy of atoms with unsaturated bonds, as shown in Supplementary Fig. 11. Such bond reconfiguration was observed to be a discrete event occurring immediately prior to catastrophic failure. Such non-progressive damage agrees well with the experimental results (Fig. 2c,d). At the macroscale, fatigue is traditionally regarded to occur due to progressive damage/plasticity[1]. However, no clear signs of progressive plasticity were observed experimentally or in atomistic simulations of monolayer graphene under cyclic loading. As a comparison, quasi-static failure of the same graphene samples (under strain rates of 10^8, 10^9 and $10^{10}\,s^{-1}$) occurred by pure bond stretching without any discernible bond reconfiguration (Supplementary Fig. 12).

In contrast, fatigue loading of GO resulted in a continuous stress reduction with increasing number of cycles (Fig. 5e and Supplementary Fig. 13) due to local and progressive damage (Fig. 5f and Supplementary Fig. 14). Small damage zones were found to grow and coalesce progressively into larger defects (colour-coded in Fig. 5f with darker green to identify defects generated in later cycles) but without catastrophic failure, unlike graphene. It is known that the epoxide functional groups endow GO with plasticity due to the epoxide-to-ether transformation under mechanical loading[14]. Applying a large static mean stress to GO initiated such a transformation and generated multiple ether groups (C–O–C) at different sites in the basal plane. It is also observed that GO fatigue damage primarily occurs at the ether groups by C–O bond breaking during cyclic straining (Supplementary Fig. 15). After fatigue damage initiation, the existence of functional groups adds resilience to fatigue crack propagation. Compared with pristine graphene, GO is more prone to initiate cracks due to the weaker intrinsic strength and defective nature induced by functionalization[38,41]; however, it is harder for the cracks to propagate during cyclic loading due to the relatively higher fracture toughness[37]. Conversely, graphene requires a larger number of cycles and longer time to activate bond breaking and to initiate bond reconfiguration; however, once the bond reconfiguration occurs, the resistance to propagation is lower and immediate fracture ensues. Despite stemming from different atomistic mechanisms, both graphene and functionalized graphene exhibit ultrahigh fatigue resistance. The global and abrupt fracture of graphene and the local and progressive damage of GO agree well with the observed experimental fracture morphology in Fig. 4a. It is noted that a complete fatigue fracture analysis of GO was not achieved due to limitations in computational power.

Outlook

This study demonstrates that the fatigue phenomenon, in which cyclic loading lowers the stress required to cause material failure, also applies to atomically thin materials. However, in contrast to macroscopic fatigue phenomena, the non-progressive nature of graphene fatigue indicates the inapplicability of conventional fatigue mechanisms. The billion-cycle lifetime of graphene demonstrates the ultrahigh dynamic reliability of graphitic 2D materials and offers fundamental insights into the widely observed fatigue enhancement in graphene-based nanocomposites. The mechanistic difference between graphene and GO fatigue demonstrates functionalization as a potential route for tuning fatigue behaviour. This fatigue testing method can also be applied to other 2D materials that are widely used in various flexible electronics applications.

Online content

Any methods, additional references, Nature Research reporting summaries, source data, extended data, supplementary information, acknowledgements, peer review information; details of author contributions and competing interests; and statements of data and code availability are available at https://doi.org/10.1038/s41563-019-0586-y.

Received: 24 May 2019; Accepted: 12 December 2019;
Published online: 20 January 2020

References

1. Suresh, S. *Fatigue of Materials* 2nd edn (Cambridge Univ. Press, 1998).
2. Schijve, J. Fatigue of structures and materials in the 20th century and the state of the art. *Int. J. Fatigue* **25**, 679–702 (2003).
3. Ramanathan, T. et al. Functionalized graphene sheets for polymer nanocomposites. *Nat. Nanotechnol.* **3**, 327–331 (2008).
4. Chen, C. et al. Graphene mechanical oscillators with tunable frequency. *Nat. Nanotechnol.* **8**, 923–927 (2013).
5. Wang, Y. et al. Wearable and highly sensitive graphene strain sensors for human motion monitoring. *Adv. Funct. Mater.* **24**, 4666–4670 (2014).
6. Yin, B. et al. Highly stretchable, ultrasensitive and wearable strain sensors based on facilely prepared reduced graphene oxide woven fabrics in an ethanol flame. *ACS Appl. Mater. Interfaces* **9**, 32054–32064 (2017).
7. Liu, N. et al. Ultratransparent and stretchable graphene electrodes. *Sci. Adv.* **3**, e1700159 (2017).
8. Kim, K. S. et al. Large-scale pattern growth of graphene films for stretchable transparent electrodes. *Nature* **457**, 706–710 (2009).
9. Yavari, F., Rafiee, M. A., Rafiee, J., Yu, Z. Z. & Koratkar, N. Dramatic increase in fatigue life in hierarchical graphene composites. *ACS Appl. Mater. Interfaces* **2**, 2738–2743 (2010).
10. Bortz, D. R., Heras, E. G. & Martin-Gullon, I. Impressive fatigue life and fracture toughness improvements in graphene oxide/epoxy composites. *Macromolecules* **45**, 238–245 (2012).
11. Rafiee, M. A. et al. Fracture and fatigue in graphene nanocomposites. *Small* **6**, 179–183 (2010).
12. Lee, C., Wei, X., Kysar, J. W. & Hone, J. Measurement of the elastic properties and intrinsic strength of monolayer graphene. *Science* **321**, 385–388 (2008).
13. Lee, G.-H. et al. High-strength chemical-vapor-deposited graphene and grain boundaries. *Science* **340**, 1073–1076 (2013).
14. Wei, X. et al. Plasticity and ductility in graphene oxide through a mechanochemically induced damage tolerance mechanism. *Nat. Commun.* **6**, 8029 (2015).
15. Cui, T. et al. Effect of lattice stacking orientation and local thickness variation on the mechanical behavior of few layer graphene oxide. *Carbon* **136**, 168–175 (2018).

16. Pyttel, B., Schwerdt, D. & Berger, C. Very high cycle fatigue—is there a fatigue limit? *Int. J. Fatigue* **33**, 49–58 (2011).
17. Dursun, T. & Soutis, C. Recent developments in advanced aircraft aluminium alloys. *Mater. Des.* **56**, 862–871 (2014).
18. Jiang, C., Zhang, H., Song, J. & Lu, Y. Digital micromirror device (DMD)-based high-cycle tensile fatigue testing of 1D nanomaterials. *Extreme Mech. Lett.* **18**, 79–85 (2018).
19. Zhang, H., Jiang, C. & Lu, Y. Low-cycle fatigue testing of Ni nanowires based on a micro-mechanical device. *Exp. Mech.* **57**, 495–500 (2017).
20. Li, P. et al. In situ transmission electron microscopy investigation on fatigue behavior of single ZnO wires under high-cycle strain. *Nano Lett.* **14**, 480–485 (2014).
21. Gao, Z., Ding, Y., Lin, S., Hao, Y. & Wang, Z. L. Dynamic fatigue studies of ZnO nanowires by in-situ transmission electron microscopy. *Phys. Status Solidi Rapid Res. Lett.* **3**, 260–262 (2009).
22. Zhang, J. Y. et al. Length scale dependent yield strength and fatigue behavior of nanocrystalline Cu thin films. *Mater. Sci. Eng. A* **528**, 7774–7780 (2011).
23. Hosseinian, E. & Pierron, O. N. Quantitative in situ TEM tensile fatigue testing on nanocrystalline metallic ultrathin films. *Nanoscale* **5**, 12532–12541 (2013).
24. Luo, X., Zhu, X. & Zhang, G. Nanotwin-assisted grain growth in nanocrystalline gold films under cyclic loading. *Nat. Commun.* **5**, 3021 (2014).
25. Sundararajan, S. & Bhushan, B. Development of AFM-based techniques to measure mechanical properties of nanoscale structures. *Sens. Actuat. A* **101**, 338–351 (2002).
26. Namazu, T. & Isono, Y. Fatigue life prediction citerion for micro-nanoscale single-crystal silicon structures. *J. Microelectromech. Syst.* **18**, 129–137 (2009).
27. Mayer, H. & Papakyriacou, M. Fatigue behaviour of graphite and interpenetrating graphite–aluminium composite up to 10^9 load cycles. *Carbon* **44**, 1801–1807 (2006).
28. Davies, A. R., Field, J. E., Takahashi, K. & Hada, K. Tensile and fatigue strength of free-standing CVD diamond. *Diam. Relat. Mater.* **14**, 6–10 (2005).
29. Banerjee, A. et al. Ultralarge elastic deformation of nanoscale diamond. *Science* **360**, 300–302 (2018).
30. Lee, C. et al. Elastic and frictional properties of graphene. *Phys. Status Solidi* **246**, 2562–2567 (2009).
31. Sakin, R. & Ay, I. Statistical analysis of bending fatigue life data using Weibull distribution in glass-fiber reinforced polyester composites. *Mater. Des.* **29**, 1170–1181 (2008).
32. Selmy, A. I., Azab, N. A. & Abd El-Baky, M. A. Flexural fatigue characteristics of two different types of glass fiber/epoxy polymeric composite laminates with statistical analysis. *Compos. B Eng.* **45**, 518–527 (2013).
33. Zhurkov, S. N. Kinetic concept of the strength of solids. *Int. J. Fract.* **26**, 295–307 (1984).
34. Tsivinsky, S. V. Thermal fluctuation theory of durability of solids. *Mater. Sci. Eng.* **26**, 13–22 (1976).
35. Santucci, S., Vanel, L., Guarino, A., Scorretti, R. & Ciliberto, S. Thermal activation of rupture and slow crack growth. *Europhys. Lett.* **62**, 320–326 (2003).
36. Phoenix, S. L. & Tierney, L. J. A statistical model for the time dependent failure of unidirectional composite materials under local elastic load-sharing among fibers. *Eng. Fract. Mech.* **18**, 193–215 (1983).
37. Cao, C. et al. Nonlinear fracture toughness measurement and crack propagation resistance of functionalized graphene multilayers. *Sci. Adv.* **4**, eaao7202 (2018).
38. Zandiatashbar, A. et al. Effect of defects on the intrinsic strength and stiffness of graphene. *Nat. Commun.* **5**, 3186 (2014).
39. Yoon, K. et al. Atomistic-scale simulations of defect formation in graphene under noble gas ion irradiation. *ACS Nano* **10**, 8376–8384 (2016).
40. Yang, Z., Huang, Y., Bao, H., Xu, K. & Ma, F. Synergistic effects of grain boundaries and edges on fatigue deformations of sub-5 nm graphene nanoribbons. *J. Mater. Sci.* **52**, 10871–10878 (2017).
41. Cao, C., Daly, M., Singh, C. V., Sun, Y. & Filleter, T. High strength measurement of monolayer graphene oxide. *Carbon* **81**, 497–504 (2015).

Methods

Materials. Graphene films were mechanically exfoliated from graphite (flaggy flakes from NGS Naturgraphit) on perforated silicon substrates with a 285 nm oxide layer following the protocol in ref. [42]. Perforated holes (2.5 μm and 1.5 μm diameter and 600 nm depth) were fabricated by electron-beam lithography followed by reactive ion etching. GO was synthesized using the improved Hummers method[43]. Previous X-ray photoelectron spectroscopy (XPS) analysis of GO samples[15] revealed ~70% oxidation with epoxide-rich functional groups, which is in good agreement with the literature for similar synthesis methods[14]. GO films were prepared by liquid-assisted chemical exfoliation[15] and dropcast on holey Si_3N_4 TEM grids to allow mechanical testing as well as TEM characterization. The number of graphene layers was determined by optical microscopy and AFM. The structure and thickness characterization of GO was conducted by scanning electron microscopy (SEM), TEM bright-field imaging and selected area electron diffraction analysis.

Experimental fatigue testing. Fatigue experiments were conducted with an Asylum MFP-3D AFM using a customized scheme as depicted in Supplementary Fig. 1a. Through actuation of a Z scanner, the centre of the film was loaded to a predefined setpoint, which corresponds to the static deflection of the cantilever (d.c. force, F_{dc}). Thereafter, the shake piezo connected to the cantilever was oscillated at a predefined drive frequency and drive amplitude (a.c. force, F_{ac}). During the static loading and oscillating process, the scan area was set to be zero, thus fixing the loading point at the centre of the film. The deflection and oscillation of the cantilever were captured by monitoring the position of the reflected laser beam on a four-quadrant photodiode. The photodiode measured the raw electrical signal change ΔV (in V) during oscillation, and the static deflection and oscillation amplitudes of the cantilever (in nm) were obtained by multiplying ΔV by the calibrated deflection and amplitude sensitivities, respectively (in nm V^{-1}). The deflection sensitivity was calibrated by deflecting the cantilever against a hard Si substrate in contact mode, and the slope of the Z (vertical) sensor displacement–voltage curve is the deflection sensitivity. The amplitude sensitivity was calibrated by measuring a force curve on the Si substrate in tapping (a.c.) mode, and the slope of the Z (vertical) sensor displacement–amplitude voltage curve is the amplitude sensitivity. The AFM used a lock-in amplifier to extract the cantilever amplitude and phase signal at the driving frequency. Based on the frequency analysis (see Supplementary Information), we believe that the AFM tip and sample are always in contact during the cyclic loading process. The cantilever oscillation amplitude can then be translated to the cyclic force range (ΔF) applied to the film, $\Delta F = k \times 2A_1$, where k is the spring constant of the cantilever and A_1 is the tip oscillation amplitude. Single-crystal diamond tips (K-TEK Nanotechnology, D160 and D300 tips) were used for both static and fatigue loading. Supplementary Fig. 1b,c presents SEM images of a used diamond tip, showing the ~20 nm of tip radius. The force ratio $F_{dc}/\bar{F}_{fracture}$ was obtained by measuring F_{dc} and $F_{fracture}$ of samples in the same flake using the same diamond tip. The average fracture force, $\bar{F}_{fracture}$, was obtained by averaging at least three samples for every flake. Furthermore, to avoid any possible tip variation on the measurement of $F_{dc}/\bar{F}_{fracture}$, static deflection measurements and fatigue measurements were conducted in an alternating sequence, rather than finishing all the static measurements and then conducting all the fatigue experiments.

The fatigue tests were conducted after one day of stabilization of the system to minimize drift. In our experiment, the drift was minimal after this stabilization period. Supplementary Fig. 1d,e presents AFM images of a graphene sample before and after 4.26 h of fatigue loading following our protocol. It shows that the drift was ~15 nm, which is less than the tip radius. The corresponding average drift rate was ~0.059 nm min^{-1}. The drift was quantified by comparing the positions of the holes in the images. The suspended graphene region was first determined by finding the threshold level of 1 nm below the substrate surface in the AFM topography image. The centroid of the two holes was then located. Overlaying the two images allowed us to measure the distance between the two centroids, which is a measure of the drift. In addition to our stabilization protocol, another characteristic of the experiments that ensured minimal drift was the high level of d.c. loading on the tip in contact with the graphene membrane, which significantly constrained the lateral drift of the contact point.

Stress estimation of monolayer graphene. A density functional theory (DFT)-based nonlinear FEA was conducted to more accurately predict the stress in graphene. Uniaxial stress–strain curves along the zigzag and armchair directions, as well as the equibiaxial stress–strain curve, were obtained using DFT calculations and then served as inputs to ABAQUS. DFT calculations were performed using the QUANTUM-ESPRESSO[44] code with the Perdew–Burke–Ernzerhof generalized gradient approximation (PBE-GGA) exchange-correlation functional[45], a uniform 13×13×3 Monkhorst–Pack k-point mesh[46] and Vanderbilt ultrasoft pseudopotential. The atomic positions and lattice constants of graphene were calculated using a kinetic energy cutoff of 60 for wavefunctions and 480 Ry for charge density, respectively. The convergence thresholds on self-consistent field (SCF) procedures and on total energy for ionic minimization between two consecutive SCF steps were 1.0×10^{-6} Ry and 1.0×10^{-4} Ry, respectively. The graphene structure, which contained four C atoms, was initially relaxed until the magnitude of the residual Hellmann–Feynman force on each atom was less than 0.001 Ry/Bohr. To simulate uniaxial tensile deformation while considering Poisson's effect, the cell dimensions in the transverse directions were allowed to relax with a variable cell relaxation. A vacuum spacing of 20 Å was used in the out-of-plane direction to avoid inter-layer interactions. The true (Cauchy) stress (σ) for prescribed levels of strain was obtained for each optimized structure from the pressure tensor. A thickness of 3.4 Å was assumed to calculate stress. The lattice parameters for the graphene unit cell (Supplementary Fig. 6a) were estimated as 2.46 Å and 4.27 Å, respectively.

Finite element simulation of graphene deflection was conducted using ABAQUS. The graphene sheet was modelled with four-node quadrilateral membrane elements (M3D4) considering the fifth-order strain energy density potential in a hyperelastic model. The indenter was modelled as a rigid body. An experimentally determined pre-stress of 0.3 N m^{-1} was applied radially on the graphene sheet. Indentation was conducted by displacing the indenter towards the centre of the membrane. The Newton–Raphson nonlinear algorithm with automatic time increment was employed to solve the problem.

MD model set-up. MD simulations were conducted using the Large-scale Atomic/Molecular Massively Parallel Simulator (LAMMPS)[47] and the interatomic interactions were computed using the ReaxFF potential[48], which has been used to successfully predict the mechanical properties of graphene and GO[38,39,49]. Based on XPS characterization, the GO monolayers were kept 70% functionalized with an epoxide-to-hydroxyl ratio of ~4:1[14,15]. The functionalized carbon atoms were chosen randomly, and identical weightages were assigned to locations on both sides of the carbon planes. For both graphene and GO, the simulation cells were kept as 7.5 nm × 7.5 nm in the in-plane directions and 11.7 nm in the out-of-plane direction. Geometric relaxation was achieved in an NPT (N, number of atoms; P, pressure; T, temperature) ensemble, in which the number of atoms, pressure and temperature were kept constant. All the structures were initially assigned a Gaussian velocity distribution and were thermally equilibrated at 300 K in an NPT ensemble. The simulation time step was 0.25 fs for GO and 1 fs for graphene, consistent with previous MD simulations[37]. Thereafter, a single C atom was removed from the centre of the structures, which were subsequently equilibrated at 300 K (Fig. 5a,d). The GO and graphene samples contained a total of 3,451 and 2,231 atoms, respectively. For the thermal relaxation of the samples, a periodic boundary condition was applied along the orthogonal directions.

MD simulations for quasi-static tensile tests. Equibiaxial strain-controlled tensile loading was imposed by dilating the simulation box along both armchair and zigzag directions. The atomic stresses of individual atoms in the GO and graphene samples were estimated using the virial theorem after every 2.5 fs for GO and 10 fs for graphene. To obtain 3D stress values, the thicknesses of the GO and graphene samples were assumed to be 6.24 and 3.4 Å, respectively. Material failure was identified by a sudden drop in tensile stress and the fracture strength (σ_f) was the maximum stress measured in the stress–strain curve. The Open Visualization Tool (Ovito) was used to visualize and capture atomic configurations[50].

MD simulations for fatigue tests. To mimic the experimental loading conditions, after equilibrating the structures at 300 K, an equibiaxial tensile mean strain was applied on the GO and graphene samples at a strain rate of 10^8 s^{-1}. The mean strain was imposed at different percentages of the quasi-static fracture strain, specifically 17, 34, 51, 68, 76 and 85% for GO and 22, 30, 44 and 55% for graphene. Once biaxially stretched, fatigue loading was imposed by sinusoidally stretching and compressing the simulation box along the in-plane directions using the expression

$$l_t = l_0 + a\sin\left(\frac{2\pi t}{T}\right)$$

where l_t is the length in any of the in-plane directions at any time t during the fatigue, l_0 is the length immediately after applying the static mean strain, a is the amplitude, t is the time and T is the period of fatigue loading. The length of the simulation box was controlled in the out-of-plane direction to maintain zero pressure. The frequency of the fatigue loading was set to 10 GHz. Due to restrictions arising from computational requirements, the frequency used in MD simulations was much larger than those in the experiments. The magnitudes of fatigue amplitude a were chosen to be 0.2, 1 and 2 Å for GO and 0.1, 0.2, 0.3, 0.4, 0.5, 0.6 and 0.8 Å for graphene oscillating at 10 GHz. For graphene oscillating at 100 GHz, the magnitude of a was chosen to be 0.6 and 0.8 Å. For all these cyclic loading simulations, the strain rates were between 1.6×10^8 s^{-1} and 5.0×10^9 s^{-1}. For long-term static dwelling simulations ($a = 0$), the samples were equibiaxially loaded under quasi-static conditions at a strain rate of 10^8 s^{-1} until the stresses reached the fatigue fracture stress values of the samples (that is, the maximum stress withstood by each sample under cyclic loading). Thereafter, they were held at those stress levels using an isothermal NVT (V, volume) ensemble for periods longer than the cyclic loading time.

Data availability

The data that support the findings of this study are available from the authors on reasonable request.

Code availability

The codes used for the fatigue data analysis in this study are available from the corresponding authors upon reasonable request.

References

42. Huang, Y. et al. Reliable exfoliation of large-area high-quality flakes of graphene and other two-dimensional materials. *ACS Nano* **9**, 10612–10620 (2015).
43. Marcano, D. C. et al. Improved synthesis of graphene oxide. *ACS Nano* **4**, 4806–4814 (2010).
44. Giannozzi, P. et al. QUANTUM ESPRESSO: a modular and open-source software project for quantum simulations of materials. *J. Phys. Condens. Matter* **21**, 395502 (2009).
45. Perdew, J. P., Burke, K. & Ernzerhof, M. Generalized gradient approximation made simple. *Phys. Rev. Lett.* **77**, 3865–3868 (1996).
46. Hendrik, J. Monkhorst. Special points for Brillouin-zone integretions. *Phys. Rev. B* **13**, 5188–5192 (1976).
47. Plimpton, S. Fast parallel algorithms for short-range molecular dynamics. *J. Comput. Phys.* **117**, 1–19 (1995).
48. Chenoweth, K., Van Duin, A. C. T. & Goddard, W. A. ReaxFF reactive force field for molecular dynamics simulations of hydrocarbon oxidation. *J. Phys. Chem. A* **112**, 1040–1053 (2008).
49. Medhekar, N. V., Ramasubramaniam, A., Ruoff, R. S. & Shenoy, V. B. Hydrogen bond networks in graphene oxide composite paper: structure and mechanical properties. *ACS Nano* **4**, 2300–2306 (2010).
50. Stukowski, A. Visualization and analysis of atomistic simulation data with OVITO—the open visualization tool. *Model. Simul. Mater. Sci. Eng.* **18**, 015012 (2010).

Acknowledgements

We acknowledge financial support from the Natural Sciences and Engineering Research Council of Canada (NSERC), the Canada Foundation for Innovation (CFI), the Erwin Edward Hart Professorship, the Ontario Ministry of Research and Innovation Early Career Researcher Award, the Canada Research Chairs Program and the Ontario Research Funds—Research Excellence programme. SEM and TEM measurements were performed at the Ontario Centre for the Characterization of Advanced Materials (OCCAM). MD simulations were performed at the SciNet and Calculquebec consortia. SciNet is funded by the Canada Foundation for Innovation under the auspices of Compute Canada, the Government of Ontario, Ontario Research Fund-Research Excellence and the University of Toronto. We thank J. Li at Asylum Research for technical assistance with experiments.

Author contributions

T.C. conceived the idea. T.F. and Y.S. supervised T.C. on the sample preparation and all the fatigue experiments. C.V.S. supervised S.M. on the MD and DFT simulations. F.N. and T.C. performed FEA. P.M.A. directed P.M.S. on GO synthesis. G.C. programmed the code for data analysis. J.T. conducted the TEM measurements. T.C. and S.M. wrote the manuscript. All authors discussed the results and analysis, and reviewed and revised the final manuscript.

Competing interests

The authors declare no competing interests.

Additional information

Supplementary information is available for this paper at https://doi.org/10.1038/s41563-019-0586-y.

Correspondence and requests for materials should be addressed to C.V.S., Y.S. or T.F.

Reprints and permissions information is available at www.nature.com/reprints.